The 130 GeV gamma-ray line and Sommerfeld enhancements

Jing Chen* and Yu-Feng Zhou†

State Key Laboratory of Theoretical Physics,
Kavli Institute for Theoretical Physics China,
Institute of Theoretical Physics, Chinese Academy of Sciences,
Beijing, 100190, China

Abstract

Recently, possible indications of line spectral features in the Fermi-LAT photon spectrum towards the galactic center have been reported. If the distinct line features arise from dark matter (DM) annihilation into γX ($X = \gamma, Z^0$ or h^0), the corresponding annihilation cross-section is unnaturally large for typical loop-induced radiative processes. On the other hand, it is still too small to be responsible for the observed DM relic density. We show that the mechanism of Sommerfeld enhancement with scalar force-carrier can provide a simple solution to these puzzles. The possibly large Sommerfeld enhancement of the cross-section for s-wave DM annihilation can significantly reduce the required effective couplings between DM and charged particles in typical loop diagrams. The DM particles necessarily annihilate into scalar force-carriers through tree-level p-wave process, which can dominate the total DM annihilation cross-section at freeze out, resulting in the correct thermal relic density, but has subdominant contributions to the DM annihilation today due to velocity suppression. We perform detailed analysis on the effects of p-wave Sommerfeld enhancement on freeze out. The results show that with the constraints from the thermal relic density, the required effective couplings can be reduced by an order of magnitude.

*Email: jchen@itp.ac.cn
†Email: yfzhou@itp.ac.cn

1 Introduction

It has been well-established from observations that dark matter (DM) contributes to nearly 23% of the energy budget of the Universe. The leading DM candidates such as the weakly interacting massive particles (WIMPs) can interact weakly with the ordinary matter and possibly be detected through direct and indirect searches. Monoenergetic gamma-ray lines are one of the smoking gun signals of halo DM annihilation, which is hard to mimic by astrophysical sources.

Recently, a possible line spectral feature around 130 GeV or with an additional line at 111 GeV in the Fermi-Large-Area-Telescope (Fermi-LAT) photon spectrum in regions close to the galactic center (GC) have been reported [1–5]. Indications of similar spectral features have been reported in the galactic clusters with modest statistical significance [6] and possibly in unassociated gamma-ray point sources [7–10]. The latest analysis from Fermi-LAT collaboration also shows the indication of such line feature at 130 GeV (135 GeV) with 4.01 (3.35) σ local significance using unreprocessed (reprocessed) data [11]. However, no globally significant gamma-ray line features have been established from the analysis of Fermi-LAT collaboration. It remains to be confirmed whether these line features are indeed from DM annihilation or due to instrumental uncertainties [12] or astrophysical backgrounds [13–15]. The upcoming HESS-II experiment can provide an independent check on existence of the gamma-ray line features.

The monoenergetic gamma-ray lines naturally arise from DM annihilation into two-body final states γX, where X stands for the Standard Model (SM) neutral particles γ, Z^0 and Higgs boson h^0 etc.. In this case, the energy of the photon is given by $E_\gamma = m_\chi[1 - m_X^2/(4m_\chi^2)]$, where m_χ is the DM mass. The observed line signals correspond to a thermally averaged cross section multiplied by relative velocity $\langle\sigma_{\gamma\gamma}v_{\rm rel}\rangle \sim 1.27\times10^{-27}$ cm^{3}s^{-1} for Einasto profile and $\sim 2.27\times10^{-27}$ cm^{3}s^{-1} for a generalized Navarro-Frenk-White (NFW) profile respectively [2]. Although the line spectral feature is expected from DM two-body annihilation, the corresponding cross-section and non-observation of an excess of accompanying continuum gamma-ray flux may challenge the explanation in terms of simple WIMP models [16–18]. First, in most DM models the DM-photon couplings are generated radiatively through loop level diagrams with charged intermediate states $F\bar{F}$ where F can be SM charged gauge bosons $W^\pm$ and charged fermions f except for the top-quark. For an annihilation cross-section $\langle\sigma_{\gamma\gamma}v_{\rm rel}\rangle \approx \mathcal{O}(10^{-27})$ cm^{3}s^{-1}, the required DM couplings to mediator particles are in general unnaturally large, which may raise the question of perturbativity [16]. Second, if the intermediate charged states are kinematically allowed to be the annihilation final states such as $f\bar{f}$ and $W^\pm W^\mp$, the corresponding tree level cross-sections are related to that of DM annihilation into 2γ as $\langle\sigma_{f\bar{f},WW}v_{\rm rel}\rangle/\langle\sigma_{\gamma\gamma}v_{\rm rel}\rangle \sim (\pi/\alpha_{\rm em})^2 \approx 2\times10^5$. Such

a large cross-section is stringently constrained by the non-observation of any excesses in the continuum gamma-ray spectrum and the cosmic-ray antiproton flux [19–23]. Finally, if the $\chi\bar{\chi} \to F\bar{F}$ channels are not opened and $\chi\bar{\chi} \to \gamma X$ is the main DM annihilation channel as suggested by the current observations, the corresponding cross-section is not large enough to generate the correct DM thermal relic density which typically requires $\langle\sigma v_{\rm rel}\rangle_F \approx 3 \times 10^{-26}$ cm^{3}s^{-1} for s-wave annihilation.

Several mechanisms have been proposed to address this problem such as co-annihilation, forbidden channel, asymmetric DM [17], resonant annihilation and cascade annihilation [18], etc.. Note that many of them introduce degeneracies in the mass of the DM particles and the intermediate particles. Specific models in which the signals of $\chi\bar{\chi} \to \gamma X$ and the thermal relic density are not correlated have been considered in Refs. [24–33].

In this work, we show that the Sommerfeld enhancement with *scalar* force-carrier can simultaneously explain the large loop level cross-sections and the correct thermal relic density without introducing degeneracies in the mass of the DM and mediator particles. In the presence of Sommerfeld enhancement, the cross-section for s-wave annihilation $\chi\bar{\chi} \to \gamma X$ today can be greatly enhanced due to the multiple exchange of a light force-carrier ϕ, which reduces the required couplings in the loop diagrams. As the force-carriers are light, the DM particles necessarily annihilate into the force-carriers. For ϕ being a scalar particle, the annihilation $\chi\bar{\chi} \to \phi\phi$ proceeds through p-wave. The p-wave process is also Sommerfeld enhanced, which can dominate the total annihilation cross-section at freeze out, lead to the correct thermal relic density, but plays a subdominant role in the halo DM annihilation today due to the velocity suppression. The total annihilation in the halo can be dominated by γX channel, which can explain both the reported gamma-ray line spectrum and the nonobservation of continuum spectrum.

This paper is organized as follows. In Sec. 2, we begin with a brief review on the main features of the Sommerfeld enhancement, and then focus on the Sommerfeld enhancement of p-wave processes and its impact on the thermal relic density. The effects of kinetic decoupling for p-wave processes are also discussed. In Sec. 3, we discuss the maximally allowed Sommerfeld enhancement factor after considering the constraints from the thermal relic density for the case with scalar force-carriers. In Sec. 4, we apply the mechanism to a reference DM model in which the $\chi\bar{\chi} \to 2\gamma$ proceeds through one-loop diagrams and discuss reduction of the required effective couplings between DM particles and the charged intermediate states in the loop. The conclusions are given in Sec. 5.

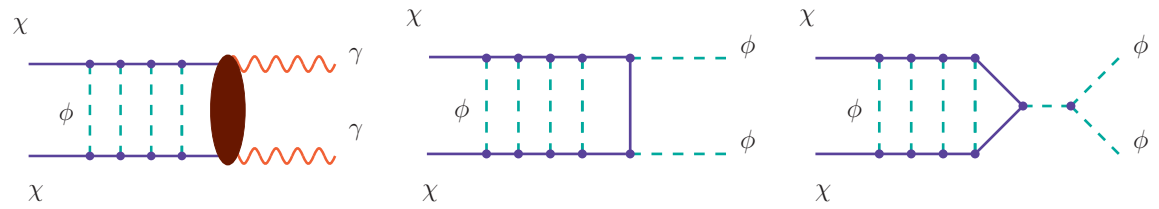

Figure 1: (Left) Feynman diagram of DM annihilation into 2γ with multiple-exchange of force-carriers which leads to the Sommerfeld enhancement; (Middle) diagram of t-channel DM annihilation into force-carrier particles; (Right) diagram of s-channel DM particle annihilation into force-carrier particles through ϕ^3 type interactions.

2 Sommerfeld enhancements of p-wave DM annihilation and thermal relic density

The Sommerfeld enhancement of annihilation cross-section occurs when the annihilating particles self-interact through a long-range attractive potential $V(\mathbf{r})$ at low velocities [34]. In this scenario, the short-distance DM annihilation cross-section can be greatly enhanced due to the distortion of the wave functions of annihilating particles at origin [35–38]. The attractive potential may originate from multiple-exchange of light force carrier particles between the annihilating DM particles as shown in Fig. 1. The nature of Sommerfeld enhancement have been extensively studied (see, e.g., Refs. [39–48]) in light of the cosmic-ray positron/electron excesses observed by PAMELA [49], ATIC [50], and Fermi-LAT [51] etc..

In the previous studies, the force-carrier ϕ is often assumed to be a vector boson, as it can be naturally light [39]. The maximally allowed enhancement factor turned out to be stringently constrained by the thermal relic density due to the additional s-wave annihilation $\chi\chi \to \phi\phi$ in the presence of the light force-carrier ϕ , which may challenge the Sommerfeld enhancement as an explanation for those excesses [47, 48, 52]. Note that the cosmic-ray lepton excesses may have astrophysical origins and may not be related to the halo DM annihilation. In this work, we shall consider the Sommerfeld enhancement as a mechanism to simultaneously account for both the possible gamma-ray line signals and the correct thermal relic density. For this purpose, we shall focus on the case of *scalar* force-carriers. Although in both the vector and scalar cases the induced long-range attractive potential is of the same Yukawa type. For a scalar force-carrier, the $\chi\bar{\chi} \to \phi\phi$ is dominated by p-wave processes, which significantly modifies the relic density constraints due to the different velocity dependencies. The two-body wave function $\Psi(\mathbf{r})$ of the

annihilating DM particles satisfies the non-relativistic Schrödinger equation

$$-\frac{1}{m_\chi}\nabla^2\Psi(\mathbf{r})+V(\mathbf{r})\,\Psi(\mathbf{r})=m_\chi v^2\Psi(\mathbf{r}), \tag{1}$$

where $v=v_{\rm rel}/2$ is the velocity of DM particle in the center-of-mass frame and $v_{\rm rel}$ is the relative velocity of the annihilating DM particles. After an expansion over angular momentum ℓ, namely, $\Psi(r,\theta)=\sum_\ell P_\ell(\cos\theta)\chi_\ell(r)/r$, the Schrödinger equation for radial wave function χ_ℓ can be written as:

$$\frac{d^2\chi_\ell(t)}{dt^2}-\left[\frac{\ell(\ell+1)}{t^2}+\frac{V(t)}{m_\chi v^2}\right]\chi_\ell(t)+\chi_\ell(t)=0, \tag{2}$$

where $t\equiv m_\chi v r$. The above Schrödinger equation can be solved with the following boundary conditions [41, 42]

$$\lim_{t\to 0}\chi_\ell(t)=t^{\ell+1}\ \text{and}\ \lim_{t\to\infty}\chi_\ell(t)\to C\sin\left(t-\frac{\ell\pi}{2}+\delta_\ell\right), \tag{3}$$

where δ_ℓ is the phase shift and C is a normalization constant. With the above boundary conditions, the Sommerfeld enhancement factor S_ℓ of the annihilation cross-section is given by [39]

$$S_\ell\equiv\lim_{t\to 0}\left|\frac{\chi_\ell(t)}{\chi_\ell^{(0)}(t)}\right|^2=\left[\frac{(2\ell+1)!!}{C}\right]^2, \tag{4}$$

where $\chi_\ell^{(0)}(t)$ is the wave function in the free-motion case without a potential. The exchange of massive vector or scalar particles ϕ between the DM particles results in an attractive Yukawa potential

$$V(r)=-\frac{\alpha e^{-m_\phi r}}{r}, \tag{5}$$

where $\alpha=g^2/(4\pi)$ is the coupling strength of $\chi\bar{\chi}\phi$ or $\bar{\chi}\gamma^\mu\chi\phi_\mu$ type of interactions. The nature of the Sommerfeld enhancement depends on the two variables

$$\epsilon_v\equiv\frac{v}{\alpha}\ \text{and}\ \epsilon_\phi\equiv\frac{m_\phi}{\alpha m_\chi}. \tag{6}$$

In the limit of $\epsilon_\phi\ll\epsilon_v^2$, the Yukawa potential can be well approximated by a Coulomb-type potential. The corresponding Schrödinger equation can be solved analytically for arbitrary angular momentum and the enhancement factors are [42]

$$S_\ell^{\rm Col}=\begin{cases}\left(\dfrac{\pi}{\epsilon_v}\right)\dfrac{1}{1-\exp\left(-\pi/\epsilon_v\right)}, & (\text{for } \ell=0),\\[2ex] S_0^{\rm Col}\cdot\displaystyle\prod_{n=1}^{l}\left(1+\frac{1}{4n^2\epsilon_v^2}\right), & (\text{for } \ell\neq 0).\end{cases} \tag{7}$$

For small $\epsilon_v/\pi \ll 1$, the enhancement factors can be approximated by $S_\ell^{\rm Col} \approx 2\pi/((2\epsilon_v)^{2\ell+1}(\ell!)^2)$. Therefore, at low velocities the s- and p-wave Sommerfeld enhancement factor scales as $1/v$ and $(1/v^3)$ respectively.

In the case where ϵ_ϕ is non-negligible, the $1/v$ behavior of s-wave cross-section breaks down. Through approximating the Yukawa potential by the Hulthén potential, the s-wave Sommerfeld enhancement factor can be estimated as [42, 43]

$$S_0 \approx \left(\frac{\pi}{\epsilon_v}\right) \frac{\sinh\left(\frac{2\pi\epsilon_v}{\pi^2\epsilon_\phi/6}\right)}{\cosh\left(\frac{2\pi\epsilon_v}{\pi^2\epsilon_\phi/6}\right) - \cos\left(2\pi\sqrt{\frac{1}{\pi^2\epsilon_\phi/6} - \frac{\epsilon_v^2}{\left(\pi^2\epsilon_\phi/6\right)^2}}\right)}. \tag{8}$$

For $\epsilon_\phi \gg \epsilon_v$, namely, the deBroglie wavelength of incoming particles is longer than the range of the interaction, the s-wave Sommerfeld enhancement saturate with $S_0 \sim 12/\epsilon_\phi$. But for some particular values of $\epsilon_\phi \simeq 6/(\pi^2 n^2), (n = 1, 2, 3, \dots)$ for which the DM can form zero-energy bound states, there exists additional resonant enhancements which scale as $1/v^2$. The resonant enhancement is eventually cut off by the finite width of the resonance [39].

For p-wave Sommerfeld enhancement factor S_1, there is no analytic expression available. The p-wave case has been investigated in Refs. [40–42] without considering its effects on the freeze out and thermal relic density. In this work, we shall focus on these effects as they are important in determining the maximally allowed Sommerfeld enhancement. We first numerically solve the Eq. (2) with the boundary conditions in Eq. (3) and illustrate the dependence of S_1 on the two variables ϵ_v and ϵ_ϕ in Fig. 2. For small $\epsilon_\phi \lesssim 10^{-3}$, the value of S_1 scales as $1/v^3$ as expected from the Coulomb limit. For larger ϵ_ϕ in the range $10^{-3} - 10^{-1}$, it has resonant behavior which is similar to the s-wave case. For even larger $\epsilon_\phi \gtrsim 10^{-1}$ the enhancement saturates. Note that the generic p-wave annihilation cross-section before including the Sommerfeld enhancement is proportional to v^2, thus the velocity dependence of the total Sommerfeld enhanced p-wave annihilation cross-section should be proportional to $S_1\epsilon_v^2$. In the right panel of Fig. 2, the contours of $S_1\epsilon_v^2$ in the $(\epsilon_v, \epsilon_\phi)$ plane are shown. In the region where $\epsilon_\phi \lesssim 10^{-3}$, it scales as $1/v$ instead of $1/v^3$. In the resonance region $10^{-3} \lesssim \epsilon_\phi \lesssim 10^{-1}$, the velocity dependence of $S_1\epsilon_v^2$ is not significant. In the saturation region $\epsilon_\phi \gtrsim 10^{-1}$, $S_1\epsilon_v^2$ scales as v^2, the total cross-section decreases rapidly towards low velocities. Thus the main difference from the s-wave case is that the total p-wave annihilation cross-section can be either velocity-suppressed or velocity-enhanced, depending on the size of ϵ_ϕ.

An important quantity directly related to the thermal relic density is thermally averaged annihilation cross-section. The generic DM annihilation cross-section times the relative velocity before including the Sommerfeld enhancement has the form $(\sigma v_{\rm rel})_0 =$

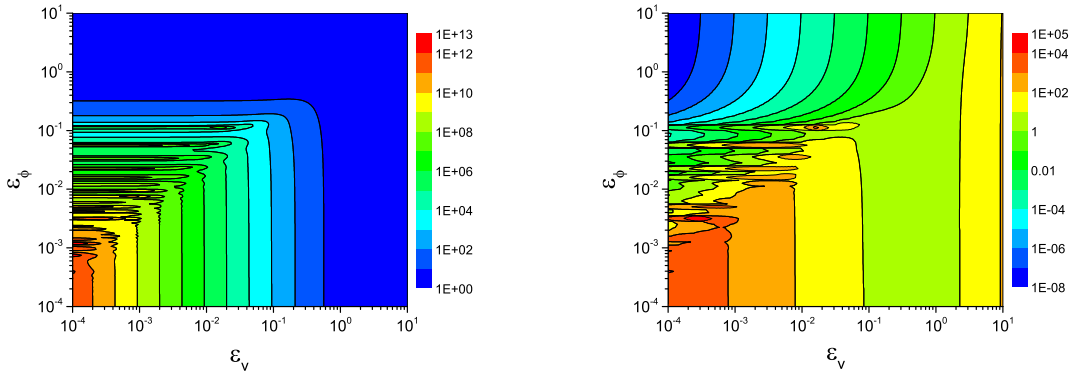

Figure 2: (Left) Contours of p-wave Sommerfeld enhancement S_1 with Yukawa potential in $(\epsilon_v, \epsilon_\phi)$ plane. (Right) the same but for $S_1\epsilon_v^2$ which is relevant to the total p-wave annihilation cross-section.

$a + bv_{\rm rel}^2 + \mathcal{O}(v_{\rm rel}^4)$, where a and b are coefficients correspond to the s- and p-wave contributions which are velocity-independent. After including the Sommerfeld enhancement, the thermally averaged cross-section at a temperature T can be written as

$$\langle \sigma v_{\rm rel} \rangle = a \langle S_0(v_{\rm rel}) \rangle + b \langle v_{\rm rel}^2 S_1(v_{\rm rel}) \rangle, \tag{9}$$

where the thermal average of a quantity $\mathcal{X}(v_{\rm rel})$ in the non-relativistic limit is given by

$$\langle \mathcal{X} \rangle = \frac{x^{3/2}}{2\sqrt{\pi}} \int_0^\infty \mathcal{X}(v_{\rm rel}) e^{-\frac{x v_{\rm rel}^2}{4}} v_{\rm rel}^2 \, dv_{\rm rel}, \tag{10}$$

with $x \equiv m_\chi / T$. The thermally averaged annihilation cross-section is a function of x and depends on the parameters α and m_ϕ.

The time evolution of the DM number density n_χ is governed by the Boltzmann equation

$$\frac{dn_\chi}{dt} + 3Hn_\chi = -\langle \sigma v_{\rm rel} \rangle \left[n_\chi^2 - (n_\chi^{\rm eq})^2 \right], \tag{11}$$

where $n_\chi^{\rm eq}$ is the equilibrium DM number density and H is the Hubble constant. The equation is often rewritten as

$$\frac{dY}{dx} = -\sqrt{\frac{\pi}{45}} m_{\rm Pl} m_\chi \frac{g_{*s} g_*^{-1/2}}{x^2} \langle \sigma v_{\rm rel} \rangle \left[Y^2 - (Y^{\rm eq})^2 \right], \tag{12}$$

where $Y^{(\rm eq)} \equiv n_\chi^{(\rm eq)}/s$ is the (equilibrium) number density rescaled by entropy density s, $m_{\rm Pl} \simeq 1.22 \times 10^{19}$ GeV is the Planck mass scale. g_{*s} and g_* are the effective relativistic degrees of freedom for entropy and energy density respectively. The decoupling temperature x_f is defined as the temperature at which the dark matter particles start to depart

from the thermal equilibrium, and the density Y is related to the equilibrium density $Y^{\rm eq}$ by $Y\left(x_f\right) \equiv (1+c)Y^{\rm eq}\left(x_f\right)$, where c is a constant of order unity. The value of x_f is approximately given by [53]

$$\begin{aligned} x_f \approx & \ln[0.038c(c+2)m_{\rm Pl}m_\chi(g_\chi g_*^{-1/2})\langle\sigma v_{\rm rel}\rangle] \\ & -\frac{1}{2}\ln\ln[0.038c(c+2)m_{\rm Pl}m_\chi(g_\chi g_*^{-1/2})\langle\sigma v_{\rm rel}\rangle], \end{aligned} \tag{13}$$

with g_χ the degrees of freedom of dark matter particle. In the absence of Sommerfeld enhancement $\langle\sigma v_{\rm rel}\rangle = a + 6b/x_f$, taking $c \approx 1(2)$ for $s(p)$-wave annihilation leads to good fits to the numerical solutions of the Boltzmann equation. The DM number density in the present-day can be obtained by integrating Eq. (12) with respect to x in the region $x_f \leq x \leq x_s$, where x_s corresponds to the temperature at which the DM annihilation rate is insignificant compared with that of the expansion of the Universe and $Y(x)$ becomes stable. The value of $Y(x_s)$ can be written as

$$\frac{1}{Y\left(x_s\right)} = \frac{1}{Y\left(x_f\right)} + \sqrt{\frac{\pi}{45}}\, m_{\rm Pl}\, m_\chi \int_{x_f}^{x_s} \frac{g_{*s}g_*^{-1/2}}{x^2}\, \langle\sigma v_{\rm rel}\rangle\, dx. \tag{14}$$

In performing the integration over x, as $\langle\sigma v_{\rm rel}\rangle$ depends on temperature, one needs to take into account the effects of kinetic decoupling. When the DM particles are in both chemical and kinetic equilibrium with the radiation background, the temperature of the DM particles tracks that of the background, i.e., $T_\chi = T$ or $x_\chi \equiv m_\chi/T_\chi = x$. After dropping out of chemical equilibrium, the DM particles can still remain in kinetic equilibrium with the radiation background through scattering off SM relativistic particles which are in thermal equilibrium with the radiation background. At some temperature $T_{\rm kd}$, when the rate of the scattering cannot compete with that of the expansion of the Universe, the DM particles start to decouple from kinetic equilibrium. After the kinetic decoupling, T_χ drops quickly with the scale factor a as a^{-2} instead of a^{-1}, the temperatures of the DM particles and the radiation background are approximately related by $T_\chi = T^2/T_{\rm kd}$, or $x_\chi = x^2/x_{\rm kd}$ [54]. Thus the integration from x_f to x_s needs to be separated into two parts, from x_f to $x_{\rm kd}$ and from $x_{\rm kd}$ to x_s. For the second part of the integration, one should use x_χ instead of x. Previous analysis have shown that including the effect of kinetic decoupling leads to a significant reduction of relic density in the case of s-wave annihilation with Sommerfeld enhancement [45, 46, 48]. The value of $T_{\rm kd}$ is model-dependent, for instance, in supersymmetric models $T_{\rm kd} \approx 10^{-3} - 10^{-1}T_f$ [55]. In this work, we shall take the value of $T_{\rm kd}$ as a free parameter. Finally, after freeze out, the relic abundance of DM particles is given by

$$\Omega h^2 \approx 2.76 \times 10^8 Y\left(x_s\right)\left(\frac{m_\chi}{\rm GeV}\right), \tag{15}$$

which is to be compared with the observed value $\Omega h^2 = 0.113 \pm 0.004$ [56].

We solve the Boltzmann equation Eq.(12) numerically including the effects of Sommerfeld enhancement and kinetic decoupling for both s-wave and p-wave annihilation. In order to facilitate the comparison, we take $a = 2.2 \times 10^{-26}$ cm^{3}s^{-1} and $b = 1.7 \times 10^{-25}$ cm^{3}s^{-1} such that the final DM relic abundance $\Omega h^2 \approx 0.113$ is the same for both s-wave and p-wave in the absence of Sommerfeld enhancement and kinetic decoupling. We fix $m_\chi = 130$ GeV and $m_\phi = 0.25$ GeV and consider two different values of $\alpha = 0.1$ and 0.01, and two kinetic decoupling temperatures $T_f = 2T_{\rm kd}$ and $10T_{\rm kd}$. The evolutions of $Y(x) - Y^{eq}(x)$ as a function of x are shown in Fig. 3. For both s- and p-wave annihilation, the inclusion of Sommerfeld enhancement results in reduction of final thermal relic density by a factor of $\mathcal{O}(1)$. For $\alpha = 0.1$ the relic density is reduced by a factor of ~ 3 for s-wave annihilation while ~ 2 for p-wave case. At high temperatures $x \sim 20$, the p-wave annihilation cross-section still decreases with temperature in the presence of Sommerfeld enhancement, which leads to earlier decoupling from the thermal background and larger relic density. As it can be seen in Fig. 3, the effects of kinetic decoupling are significantly different between s- and p-wave case. For $T_f = 2T_{\rm kd}$ and $10T_{\rm kd}$, the kinetic decoupling leads to further reduction of relic density by $\sim 50\%(20\%)$ in the s-wave case. However, for p-wave case, the reduction is almost invisible for $\alpha = 0.1$ as shown in Fig. 3. For smaller $\alpha = 0.01$, it even leads to a slight enhancement of the relic density. This is because the kinetic decoupling makes the DM particle freeze out more quickly in the p-wave case as the annihilation cross-section decreases with temperature.

3 Sommerfeld enhancement of $\chi\bar{\chi} \to \gamma X$ cross-sections

With the main features of p-wave Sommerfeld enhancement given in the previous section, we are ready to discuss the contribution to the DM thermal relic density from the process of DM particles annihilating into scalar force-carriers through p-wave. Since the force-carrier is much lighter than the DM particle, i.e., $m_\phi \ll m_\chi$, the DM particles necessarily annihilate into the force-carriers, which contributes to a DM annihilation channel in addition to γX, and can be the dominant contribution to the total DM annihilation cross-section. The process itself is also Sommerfeld-enhanced, which complicates the calculations.

Before including the effects of Sommerfeld enhancements, the total DM annihilation cross-section $(\sigma_{\rm tot} v_{\rm rel})_0$ can be written as

$$(\sigma_{\rm tot} v_{\rm rel})_0 = (\sigma_{\phi\phi} v_{\rm rel})_0 + (\sigma_{\gamma X} v_{\rm rel})_0. \tag{16}$$

The DM particles can always pair-annihilate into $\phi\phi$ through t-channel χ-exchange. In addition, if there exists non-negligible cubic and quartic self-interactions between the

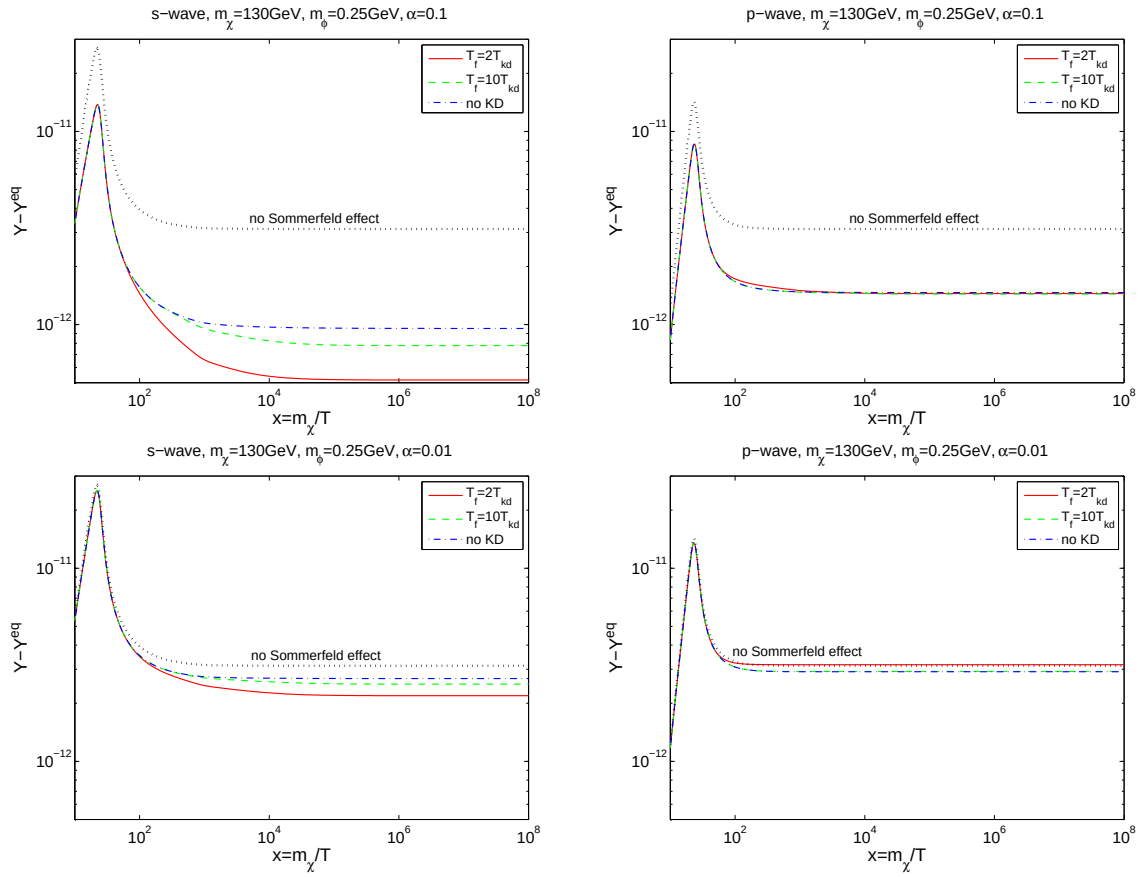

Figure 3: Effects of Sommerfeld enhancement and kinetic decoupling on the temperature evolution of the DM number density for the case of s-wave (left) and p-wave (right) with α =0.1 and 0.01, see text for explanations.

force-carriers of the form $-\mu\phi^3/3! - \lambda\phi^4/4!$, two-body or three-body s-channel annihilation may occur. The three-body annihilation is highly suppressed by small phase-space and is neglected in this work. In the case of scalar force-carrier, both the t- and s-channel two-body annihilation into $\phi\phi$ corresponding to the two diagrams in Fig. 1 are p-wave processes. In the limit of $m_\phi \ll m_\chi$, the total annihilation cross-section of $\chi\bar{\chi} \to \phi\phi$ from the calculation of the two diagrams in Fig. 1 is independent of m_ϕ, and is given by

$$(\sigma_{\phi\phi} v_{\rm rel})_0 = \frac{3\pi\alpha^2}{8m_\chi^2}\left(1 - \frac{5}{18}\xi + \frac{1}{48}\xi^2\right) v_{\rm rel}^2, \tag{17}$$

with $\xi = \mu/(2m_\chi\sqrt{\alpha\pi})$. The first term in the right-hand-side of Eq. (17) comes from the t-channel contribution. The term proportional to ξ^2 corresponds to the squared amplitude of s-channel annihilation, and the term proportional to ξ corresponds to the interference between s- and t-channel diagrams. We assume that the other annihilation channel $\chi\bar{\chi} \to \gamma X$ is an s-wave process such that there is no explicit velocity dependence

in $(\sigma_{\gamma X} v_{\rm rel})_0$. After including the Sommerfeld enhancement, the total thermally averaged annihilation cross-section is

$$\langle \sigma_{\rm tot} v_{\rm rel} \rangle = (\sigma_{\gamma X} v_{\rm rel})_0 \langle S_0 \rangle + \langle (\sigma_{\phi\phi} v_{\rm rel})_0 S_1 \rangle. \tag{18}$$

The Sommerfeld enhancement factors $S_{0,1}$ depend on parameters α and m_ϕ, and the cross-section $(\sigma_{\phi\phi} v_{\rm rel})_0$ is also a function of α. Therefore, the requirement of reproducing the correct thermal relic density determines the size of α for a given $(\sigma_{\gamma X} v_{\rm rel})_0$ and force-carrier mass m_ϕ. Using the value of α constrained by the thermal relic density, one can calculate the allowed Sommerfeld enhancement factor $\langle S_0 \rangle$ for $(\sigma_{\gamma X} v_{\rm rel})_0$ at low temperatures, which is needed to predict the cross-section of $\chi\bar{\chi} \to \gamma X$ in the present day.

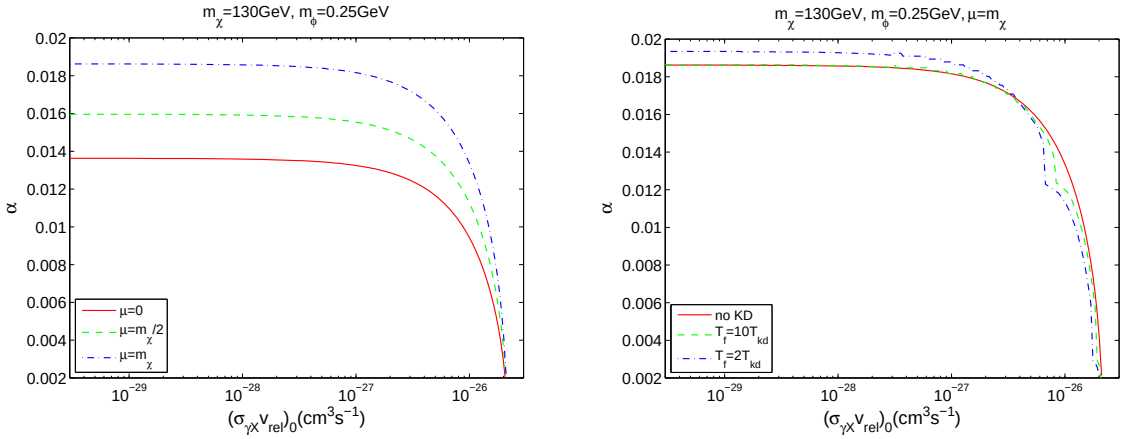

Figure 4: The value of α allowed by the DM thermal relic density as a function of $(\sigma_{\gamma X} v_{\rm rel})_0$. (Left) the cases without kinetic decoupling. Three curves correspond to $\mu = 0$ (solid), $m_\chi/2$ (dashed), and m_χ (dot-dashed), respectively. (Right) the case with kinetic decoupling. Three curves correspond to without kinetic decoupling (solid), $T_{\rm kd} = T_f/10$ (dashed) and $T_f/2$ (dot-dashed), respectively with μ fixed at m_χ.

In the left panel of Fig. 4, we show the allowed values of α as a function of $(\sigma_{\gamma X} v_{\rm rel})_0$ for a fixed $m_\phi = 0.25$ GeV with three different choices of cubic coupling μ. For sufficiently small $(\sigma_{\gamma X} v_{\rm rel})_0 \ll 10^{-26}$ cm^{3}s^{-1}, namely, the total annihilation cross-section is dominated by $(\sigma_{\phi\phi} v_{\rm rel})_0$ at freeze out, the value of α is found to be insensitive to $(\sigma_{\gamma X} v_{\rm rel})_0$. From the figure, one obtains $\alpha \approx 0.014$, 0.016, and 0.019 for $\mu = 0$, $m_\chi/2$, and m_χ, respectively. When $(\sigma_{\gamma X} v_{\rm rel})_0$ grows and approaches $\sim 10^{-26}$ cm^{3}s^{-1}, the value of $(\sigma_{\phi\phi} v_{\rm rel})_0$ needs to be suppressed in order to give the correct relic density, which results in a significant reduction of α. As it can be seen from the figure, at $(\sigma_{\gamma X} v_{\rm rel})_0 \approx 10^{-26}$ cm^{3}s^{-1}, the allowed values of α is reduced by $\sim 50\%$.

The effects of kinetic decoupling are shown in the right panel of Fig. 4 for two different decoupling temperatures $T_f = 2T_{\rm kd}$ and $10T_{\rm kd}$. For small $(\sigma_{\gamma X} v_{\rm rel})_0 \ll 10^{-26}$ cm^{3}s^{-1}, the inclusion of kinetic decoupling only leads to a slight increase of α, which is expected as in this region the p-wave annihilation dominates, the kinetic decoupling makes DM particle freeze out more quickly, which leads to a higher relic density as discussed in the previous section. For large $(\sigma_{\gamma X} v_{\rm rel})_0 \sim 10^{-26}$ cm^{3}s^{-1}, the effect of kinetic decoupling is sizeable, as in this region, the s-wave annihilation becomes important, which has a stronger dependence on the kinetic decoupling than that of p-wave case. This leads to a significant decrease of α. Especially in the vicinity of resonances, due to the additional s-wave resonant Sommerfeld enhancement, there could be a sudden reduction on the size of α, which can be seen at $(\sigma_{\gamma X} v_{\rm rel})_0 \sim 6 \times 10^{-27}$ cm^{3}s^{-1} in Fig. 4.

After constraining the allowed values of α, the s-wave Sommerfeld enhancements factor $\langle S_0 \rangle$ at low temperatures can be calculated straightforwardly. The velocity-averaged Sommerfeld enhancement of the halo DM annihilation cross-section in the present-day is defined as

$$\langle S_0 \rangle_{\rm now} = \frac{1}{N v_0^3} \sqrt{\frac{2}{\pi}} \int_0^{v_{\rm esc}} S_0 \; e^{-\frac{v_{\rm rel}^2}{2 v_0^2}} v_{\rm rel}^2 dv_{\rm rel} \; , \tag{19}$$

where v_0 is the DM velocity dispersion and v_{esc} is the DM escape velocity, respectively. $N = {\rm erf}\left(z/\sqrt{2}\right) - (2/\pi)^{1/2} z e^{-z^2/2}$ is a normalization constant with $z = v_{\rm esc}/v_0$. Both v_{esc} and v_0 depend on the distance r from the GC. In the vicinity of the Sun, $r = r_\odot \approx 8.5$ kpc, $v_{\rm esc}(r_\odot) \approx 525$ km s^{-1}, and $v_0(r_\odot) \approx 210$ km s^{-1}. In the left panel of Fig. 5, we show the dependences of $\langle S_0 \rangle_{\rm now}$ on the coupling α and the velocity dispersion v_0. For the allowed values $\alpha = 0.0136$, 0.0159, and 0.0186 corresponding to $\mu = 0$, $m_\chi/2$, and m_χ, the enhancement factors are $\langle S_0 \rangle_{\rm now} \approx 170$, 70, and 50, respectively. Thus the Sommerfeld enhancement factor can reach $\mathcal{O}(100)$ with the constraints from DM thermal relic density, which is larger than the case where the force-carrier is a vector boson [47, 48].

We are now in the position to discuss the line spectral shape in the photon spectrum recently observed by the Fermi-LAT collaboration. The observation, if interpreted as DM annihilation into $\gamma\gamma$, corresponds to an s-wave velocity-averaged cross-section $\langle \sigma_{\gamma\gamma} v_{\rm rel} \rangle_{\rm now} \sim 10^{-27}$cm^{3}s^{-1}. All of our previous results on the annihilation $\chi\bar{\chi} \to \gamma X$ can be directly applied to the case of $\chi\bar{\chi} \to \gamma\gamma$, as it is a special case of γX. In the right panel of Fig. 5, the relation between $\langle \sigma_{\gamma\gamma} v_{\rm rel} \rangle_{\rm now}$ and $(\sigma_{\gamma\gamma} v_{\rm rel})_0$ is shown. One sees that in order to reproduce the observed signal corresponding to $\langle \sigma_{\gamma\gamma} v_{\rm rel} \rangle_{\rm now} \approx 1.27 \times 10^{-27}$cm^{3}s^{-1} for the Einasto profile [2], the required cross-sections before the Sommerfeld enhancement can be quite small $(\sigma_{\gamma\gamma} v_{\rm rel})_0 = 7.2 \times 10^{-30}$ cm^{3}s^{-1}, 1.8×10^{-29} cm^{3}s^{-1}, and 2.5×10^{-29} cm^{3}s^{-1}, for $\mu = 0$, $m_\chi/2$, and m_χ, respectively.

The cross-section of $\chi\bar{\chi} \to \gamma\gamma$ may be further enhanced due to the possible lower DM

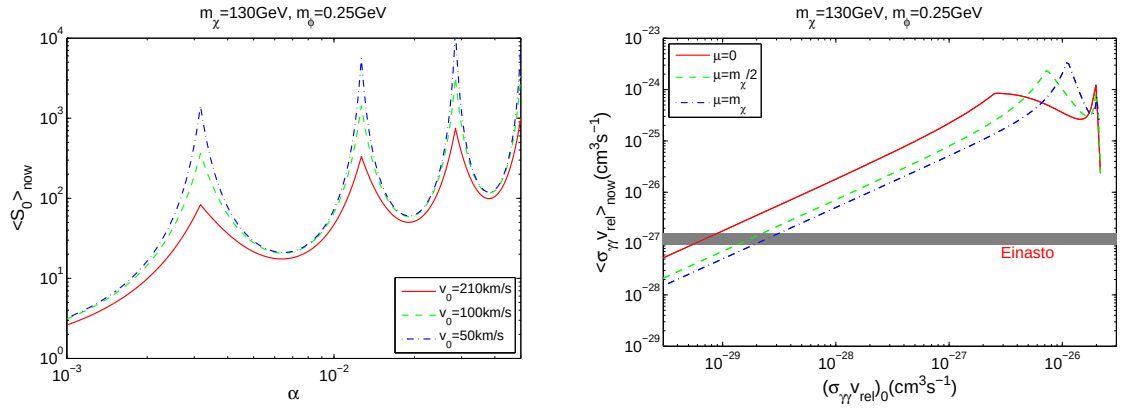

Figure 5: (Left) $\langle S_0\rangle_{\rm now}$ as a function of coupling strength α for the velocity dispersion $v_0 = 210$ km s^{-1}, 100 km s^{-1}, and 50 km s^{-1} respectively. (Right) the relation between $\langle\sigma_{\gamma\gamma}v_{\rm rel}\rangle_{\rm now}$ and $(\sigma_{\gamma\gamma}v_{\rm rel})_0$ for three different values of μ. The gray band denotes the fit cross-section $\langle\sigma_{\gamma\gamma}v\rangle = (1.27 \pm 0.32) \times 10^{-27}$ cm^{3}s^{-1} in the case of Einasto profile [2]. Other parameters are fixed at $m_\chi = 130$ GeV and $m_\phi = 0.25$ GeV.

velocity dispersion near the GC than that in the solar neighborhood. The dependence of Sommerfeld enhancement on $v_0(r)$ at GC has been discussed in Refs. [57, 58]. The N-body simulations suggest that $v_0(r)$ is related to the DM density profile $\rho(r)$ through a relation $v_0(r)^3/\rho(r) \approx r^\chi$ [59]. From pure DM simulations, the power index is found to be $\chi \simeq 1.9 - 2.0$ [60]. For the NFW profile $\rho(r) \propto (r/r_s)^{-\alpha}(1 + r/r_s)^{-3+\alpha}$ with $\alpha = 1.0$ and $r_s = 20$ kpc, $v_0(r)$ scales as $r^{\chi-\alpha}$. Therefore it decreases with the distance r. This is also true for the Einasto profile $\rho(r) \propto \exp[-(2/\alpha)(r/r_s)^\alpha]$, if one takes the typical value of $\alpha = 0.17$. Thus a larger s-wave Sommerfeld enhancement at GC can be expected. However, if the Sommerfeld enhancement saturates at some velocity smaller than $v_0(r_\odot)$, then it is insensitive to the choice of $v_0(r)$. The additional enhancement at GC in this case can be simply estimated as $S_0(v = 0)/S_0(v_0(r_\odot))$ [61]. Note that the simulation results can be modified significantly after including baryons [62].

Although at freeze out the p-wave cross-section $\langle\sigma_{\phi\phi}v_{\rm rel}\rangle$ can be a few order of magnitudes larger than the s-wave cross-section $\langle\sigma_{\gamma\gamma}v_{\rm rel}\rangle$, at lower temperatures it is possible that $\langle\sigma_{\phi\phi}v_{\rm rel}\rangle$ becomes comparable with or even smaller than $\langle\sigma_{\gamma\gamma}v_{\rm rel}\rangle$, which is due to the dramatic difference in velocity-dependencies between s- and p-wave processes in the presence of Sommerfeld enhancement. This possibility is shown in Fig. 6. At the temperature of thermal decoupling $x \approx 25$, one sees that $\langle\sigma_{\phi\phi}v_{\rm rel}\rangle \approx 1 \times 10^{-25}$ cm^{3}s^{-1} which is about four order of magnitudes larger than $\langle\sigma_{\gamma\gamma}v_{\rm rel}\rangle$. When the temperature goes down, in general the value of $\langle\sigma_{\phi\phi}v_{\rm rel}\rangle$ decreases due to the velocity-suppression. The p-wave Sommerfeld enhancement of $\langle\sigma_{\phi\phi}v_{\rm rel}\rangle$ can be significant in the range $10^4 \lesssim x \lesssim 10^6$ when

it is near a resonance region. But for other values of x which are off the resonance, $\langle\sigma_{\phi\phi}v_{\rm rel}\rangle$ decrease rapidly. On the other hand, the size of $\langle\sigma_{\gamma\gamma}v_{\rm rel}\rangle$ increases monotonically towards larger x due to the s-wave Sommerfeld enhancement. At $x \approx 25$, the value of $\langle\sigma_{\gamma\gamma}v_{\rm rel}\rangle$ is $\sim 10^{-29}$ cm^{3}s^{-1}, but at $x \approx 4\times10^6$ which corresponds to $v_0 = 210$ km s^{-1}, it reaches $\sim 10^{-27}$ cm^{3}s^{-1} and becomes comparable with $\langle\sigma_{\phi\phi}v_{\rm rel}\rangle$ for $\mu = m_\chi/2$ and m_χ. For $\mu = 0$ case, it can even dominate over $\langle\sigma_{\phi\phi}v_{\rm rel}\rangle$. Therefore, it is possible that $\chi\bar{\chi} \to \gamma\gamma$ can be the main DM annihilation channel today, and is responsible for the observed gamma-ray line at the GC. In this work, we consider a light scalar with $m_\phi \approx 0.25$ GeV, such that ϕ can decay into $\mu^+\mu^-$ and e^+e^-. But the final states of $\pi^0\pi^0$ and $\tau^+\tau^-$ are kinematically forbidden, which will suppress the generation of large continuum gamma-ray flux from the annihilation $\chi\bar{\chi} \to \phi\phi$ followed by the decay of ϕ into these final states.

Note that such a large s-wave enhancement of $\mathcal{O}(100)$ is still consistent with the limits derived from BBN and CMB data [63], as the total DM annihilation cross-section after the Sommerfeld enhancement is still an order of magnitude smaller than the typical WIMP annihilation cross-section.

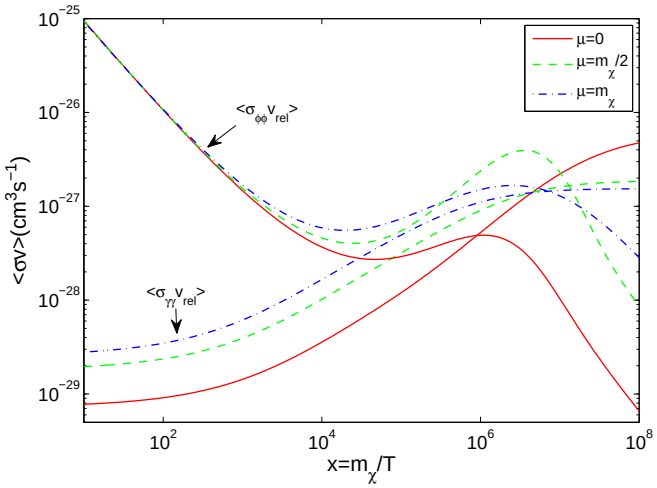

Figure 6: Temperature evolution of $\langle\sigma_{\phi\phi}v_{\rm rel}\rangle$ and $\langle\sigma_{\gamma\gamma}v_{\rm rel}\rangle$ for three different values of $\mu = 0$, $m_\chi/2$, and m_χ, respectively.

4 Sommerfeld enhancement in a simple model

We have shown in the previous section that the Sommerfeld-enhanced cross-section $\langle\sigma_{\gamma\gamma}v_{\rm rel}\rangle \sim 10^{-27}$ cm^{3}s^{-1} today can be consistent with the DM thermal relic density, due to the p-wave annihilation of DM particles into the force-carriers. In this section,

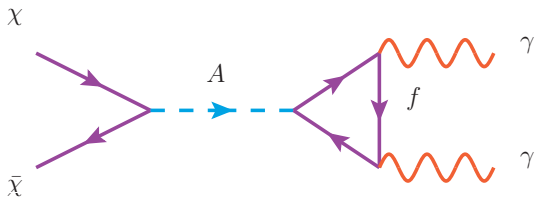

Figure 7: Feynman diagram for $\chi\bar{\chi} \to \gamma\gamma$ through loop diagrams with an intermediate pseudoscalar A^0 and a charged fermion f in the loop.

we discuss another advantage of the Sommerfeld enhancement, namely, it can also solve the problem of unnaturally large couplings required by many DM models motivated to explain the putative gamma-ray line. As the DM particles carry no electric charge, it is often assumed that the annihilation of DM particles into $\gamma\gamma$ proceeds only through one-loop diagrams which involve massive charged particles running in the loop (for exceptions, see e.g. Refs. [64, 65]). Due to the loop suppression, in general the effective DM couplings to the charged particles in the loop have to be above order unity, in order to give the cross-section suggested by Fermi-LAT (see e.g. [16]), which may raise the issue of perturbativity. Invoking the mechanism of Sommerfeld enhancements can significantly reduce the required couplings to the perturbative region.

For a concrete illustration, we consider a realization of Sommerfeld enhancement in a simple reference model. In this model, the DM particle χ is assumed to be a Majorana fermion. Other particles in the models are: a light scalar force-carrier ϕ, a heavy pseudoscalar mediator A^0, and a heavy charged Dirac fermion f with electromagnetic charge number Q_f and color number C_f. The relevant interactions in the model are given by the following Lagrangian

$$\mathcal{L}_{int} \subset -\frac{g}{2}\bar{\chi}\phi\chi - i\frac{g_\chi}{2}\bar{\chi}\gamma_5\chi A^0 - ig_f\bar{f}\gamma_5 f A^0. \tag{20}$$

In order to avoid constraints from the nonobservation of continuum photon spectrum, we consider the case where $m_f, m_A \gg m_\chi$, such that $\chi\bar{\chi} \to f\bar{f}, A^0A^0$ are kinematically forbidden, and $\chi\bar{\chi}$ can only annihilate into $\gamma\gamma$ through loop process. The corresponding Feynman diagram is shown in Fig. 7. The annihilation cross-section for this process is given by [17]

$$(\sigma_{\gamma\gamma}v_{\rm rel})_0 = \frac{1}{4\pi^3}\frac{\alpha_{\rm em}^2 g_\chi^2 g_f^2 Q_f^4 C_f^2 m_f^2}{(s-m_A^2)^2 + m_A^2\Gamma_A^2}\left[\arctan\left(\frac{1}{\sqrt{m_f^2/m_\chi^2 - 1}}\right)\right]^4, \tag{21}$$

where s is the center-of-mass total energy. The total width Γ_A of the pseudoscalar A^0 receives contribution from the decay channels $A^0 \to \chi\bar{\chi}$, $f\bar{f}$, and $\gamma\gamma$ with the partial

widths

$$\Gamma_{\chi\bar{\chi}} = \frac{g_\chi^2 m_A}{16\pi}\sqrt{1-\frac{4m_\chi^2}{m_A^2}},\ \Gamma_{f\bar{f}} = \frac{g_f^2 m_A}{8\pi}\sqrt{1-\frac{4m_f^2}{m_A^2}}, \tag{22}$$

and

$$\Gamma_{\gamma\gamma} = \frac{m_A^3 \alpha_{em}^2 g_f^2 Q_f^4 C_f^2}{256\pi^3 m_f^2}|A_{1/2}^A(m_A^2/4m_f^2)|^2, \tag{23}$$

where the function $A_{1/2}^A$ is defined as $A_{1/2}^A(\tau) = 2\tau^{-1}f(\tau)$ with

$$f(\tau) = \begin{cases} \arcsin^2\sqrt{\tau} & (\text{for } \tau \leq 1) \\ -\frac{1}{4}\left(\ln\frac{1+\sqrt{1-1/\tau}}{1-\sqrt{1-1/\tau}} - i\pi\right)^2 & (\text{for } \tau > 1) \end{cases}.$$

We assume that in the dark sector the parity symmetry is conserved such that the decay $A^0 \to \phi\phi$ is forbidden. Since A^0 is a pseudoscalar, the annihilation $\chi\bar{\chi} \to \gamma\gamma$ proceeds through s-wave. For heavy m_A, $m_f \gg m_\chi$, the size of the annihilation cross-section can be estimated as

$$(\sigma_{\gamma\gamma}v_{\rm rel})_0 \sim 10^{-27}{\rm cm}^3{\rm s}^{-1}\left(\frac{g_\chi g_f}{100}\right)^2\left(\frac{m_\chi}{130\ {\rm GeV}}\right)^4\left(\frac{500\ {\rm GeV}}{m_A}\right)^4\left(\frac{500\ {\rm GeV}}{m_f}\right)^2. \tag{24}$$

One sees that a very large product of the couplings $\sqrt{g_\chi g_f} \sim 10$ is required, which is unnatural and can invalidate the perturbative calculations. This is a common problem in many dark matter models in which the DM annihilation into $\gamma\gamma$ through one-loop diagrams.

One way to enhance the cross-section is to assume that the annihilation is near a resonance which occurs if $m_A \approx 2m_\chi + \delta$ with $\delta \ll m_A$. In this case the cross-section can be enhanced by a factor of $m_A^2/(4\delta^2 + \Gamma_A^2)$. If small couplings $g_\chi, g_f \approx 1$ is required, the relative mass difference should be around $\delta/m_A \approx 2\%$ for $\Gamma_A \approx \Gamma_{\chi\bar{\chi}}$. Another modest enhancement may arise from the case where $m_\chi \approx m_f$ such that the function $\arctan[(m_f^2/m_\chi^2 - 1)^{-1/2}]$ reaches its maximal value $\pi/2$. Compared with the case where $m_f \approx 5m_\chi$ the enhancement of the value of the arctan is ~ 8. In addition, in order to have the correct relic density, it is required that δ must be positive [18].

With the presence of Sommerfeld enhancements, the required couplings can be reduced significantly without introducing any mass degeneracies. In Fig. 8, we show the required couplings which can reproduce the observed $\langle\sigma_{\gamma\gamma}v_{\rm rel}\rangle = 1.27 \times 10^{-27}\ {\rm cm}^3{\rm s}^{-1}$. Compared with the case without Sommerfeld enhancements, the required products $g_\chi g_f$ can be reduced by an order of magnitude. For a wide range of the pseudoscalar mass $100 < m_A < 450$ GeV, the required couplings are smaller than unity. If the Sommerfeld enhancements are absent, only a narrow region close to $2m_\chi$ can be consistent with a small $g_\chi g_f$.

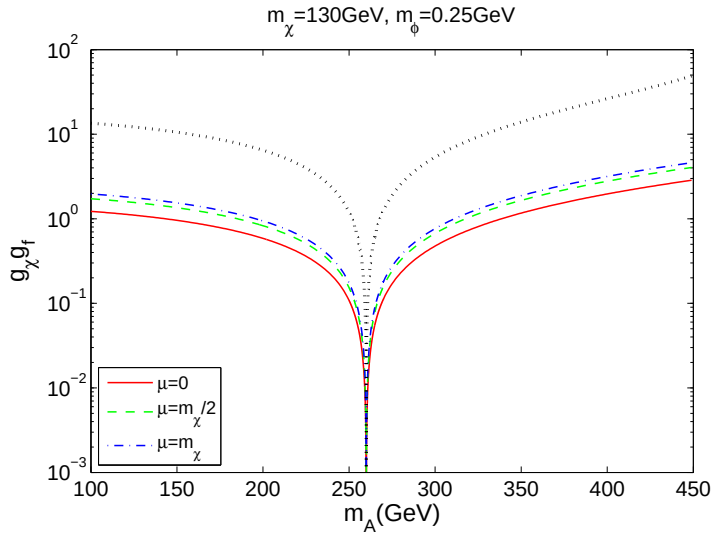

Figure 8: The required value of $g_\chi g_f$ to account for the gamma-ray line signals with cross-section $\langle\sigma_{\gamma\gamma}v_{\rm rel}\rangle = 1.27\times10^{-27}{\rm cm}^3{\rm s}^{-1}$ [2]. Three cases with Sommerfeld enhancement correspond to $\mu = 0$ (solid), $m_\chi/2$ (dashed), and m_χ (dot-dashed), respectively. The dotted line denotes the case without Sommerfeld enhancement. Other parameters are fixed at $Q_f = C_f = 1$, $g_\chi = g_f$, and $m_f = 300$ GeV.

In this simple model, the force-carrier ϕ does not appear in the leading one-loop diagram for $\chi\bar{\chi}\to\gamma\gamma$, which make it straightforward to factorize the short- and long-distance contributions. In general, the force-carrier can play important roles in both the one-loop diagram and the long-distance Sommerfeld enhancements. For instance, in the case where the DM particle is a Majorana fermion belonging to the adjoint presentation of $SU(2)_W$ gauge group (e.g Wino neutralino), the $SU(2)_W$ gauge bosons $W^\pm$ appear in both the box-diagrams for DM annihilation into $\gamma\gamma$ and the long-distance ladder diagrams as a force-carrier which results in off-diagonal Sommerfeld enhancements [35–38, 44, 66]. A fully consistent analysis of incorporating these two contribution simultaneously can be found in Ref. [67].

5 Conclusions

In summary, the recently reported possible indications of line spectral features in the Fermi-LAT photon spectrum in regions close to the galactic center can be related to the signals of halo DM annihilation. However, the corresponding annihilation cross-section of $\langle\sigma_{\gamma\gamma}v_{\rm rel}\rangle \approx \mathcal{O}(10^{-27})$ cm^{3}s^{-1} is too large for typical loop-induced radiative processes, while on the other hand too small to be responsible for the observed DM relic density

which is typically 3×10^{-26} cm^{3}s^{-1}. We have pointed out that the Sommerfeld enhancement with scalar force-carrier can simultaneously explain those features. In this mechanism, the cross-section for DM annihilation into γX in the galactic center today can be greatly enhanced due to the attractive forces between the DM particles, which is induced by the multiple-exchange of the force-carriers. The additional p-wave annihilation into the force-carriers can dominate the total DM annihilation cross-section at freeze out and set the correct thermal relic density, but can have subdominant contributions to the DM annihilation today due to the velocity suppression. We have performed an detailed analysis on the allowed Sommerfeld enhancement under the constraints from the thermal relic density determined by p-wave annihilation processes. The results show that the Sommerfeld enhancement factor can reach $\mathcal{O}(100)$. In a simple reference model with $\chi\bar{\chi} \to 2\gamma$ occurring at one loop, we have shown that the required DM effective couplings to the intermediate particles in the loop can be reduced by an order of magnitude and below unity, which keeps the perturbativity of the model. Compared with some other mechanisms for increasing the DM annihilation cross-section at loop level, the Sommerfeld enhancement does not require any degeneracies in the masses of DM particles and the intermediate particles in the loop diagrams.

Acknowledgments

This work is supported in part by the National Basic Research Program of China (973 Program) under Grants No. 2010CB833000; the National Nature Science Foundation of China (NSFC) under Grants No. 10975170, No. 10821504 and No. 10905084; and the Project of Knowledge Innovation Program (PKIP) of the Chinese Academy of Science.

References

[1] T. Bringmann, X. Huang, A. Ibarra, S. Vogl, and C. Weniger, *Fermi LAT Search for Internal Bremsstrahlung Signatures from Dark Matter Annihilation*, *JCAP* **1207** (2012) 054, [arXiv:1203.1312].

[2] C. Weniger, *A Tentative Gamma-Ray Line from Dark Matter Annihilation at the Fermi Large Area Telescope*, *JCAP* **1208** (2012) 007, [arXiv:1204.2797].

[3] E. Tempel, A. Hektor, and M. Raidal, *Fermi 130 GeV gamma-ray excess and dark matter annihilation in sub-haloes and in the Galactic centre*, *JCAP* **1209** (2012) 032, [arXiv:1205.1045].

[4] A. Rajaraman, T. M. Tait, and D. Whiteson, *Two Lines or Not Two Lines? That is the Question of Gamma Ray Spectra*, *JCAP* **1209** (2012) 003, [arXiv:1205.4723].

[5] M. Su and D. P. Finkbeiner, *Strong Evidence for Gamma-ray Line Emission from the Inner Galaxy*, arXiv:1206.1616.

[6] A. Hektor, M. Raidal, and E. Tempel, *An evidence for indirect detection of dark matter from galaxy clusters in Fermi-LAT data*, arXiv:1207.4466.

[7] M. Su and D. P. Finkbeiner, *Double Gamma-ray Lines from Unassociated Fermi-LAT Sources*, arXiv:1207.7060.

[8] D. Hooper and T. Linden, *Are Lines From Unassociated Gamma-Ray Sources Evidence For Dark Matter Annihilation?*, arXiv:1208.0828.

[9] A. Hektor, M. Raidal, and E. Tempel, *Double gamma-ray lines from unassociated Fermi-LAT sources revisited*, arXiv:1208.1996.

[10] N. Mirabal, *The Dark Knight Falters*, arXiv:1208.1693.

[11] Fermi-LAT Collaboration, http://fermi.gsfc.nasa.gov/science/mtgs/symposia/2012/program/fri/AAlbert.pdf, The Fermi Symposium, October 2012.

[12] A. Boyarsky, D. Malyshev, and O. Ruchayskiy, *Spectral and spatial variations of the diffuse gamma-ray background in the vicinity of the Galactic plane and possible nature of the feature at 130 GeV*, arXiv:1205.4700.

[13] F. Aharonian, D. Khangulyan, and D. Malyshev, *Cold ultrarelativistic pulsar winds as potential sources of galactic gamma-ray lines above 100 GeV*, arXiv:1207.0458.

[14] A. Hektor, M. Raidal, and E. Tempel, *Fermi-LAT gamma-ray signal from Earth Limb, systematic detector effects and their implications for the 130 GeV gamma-ray excess*, arXiv:1209.4548.

[15] D. P. Finkbeiner, M. Su, and C. Weniger, *Is the 130 GeV Line Real? A Search for Systematics in the Fermi-LAT Data*, arXiv:1209.4562.

[16] M. R. Buckley and D. Hooper, *Implications of a 130 GeV Gamma-Ray Line for Dark Matter*, *Phys.Rev.* **D86** (2012) 043524, [arXiv:1205.6811].

[17] S. Tulin, H.-B. Yu, and K. M. Zurek, *Three Exceptions for Thermal Dark Matter with Enhanced Annihilation to $\gamma\gamma$*, arXiv:1208.0009.

[18] Y. Bai and J. Shelton, *Gamma Lines without a Continuum: Thermal Models for the Fermi-LAT 130 GeV Gamma Line*, *JHEP* **1212** (2012) 056, [arXiv:1208.4100].

[19] W. Buchmuller and M. Garny, *Decaying vs Annihilating Dark Matter in Light of a Tentative Gamma-Ray Line*, *JCAP* **1208** (2012) 035, [arXiv:1206.7056].

[20] T. Cohen, M. Lisanti, T. R. Slatyer, and J. G. Wacker, *Illuminating the 130 GeV Gamma Line with Continuum Photons*, *JHEP* **1210** (2012) 134, [arXiv:1207.0800].

[21] I. Cholis, M. Tavakoli, and P. Ullio, *Searching for the continuum spectrum photons correlated to the 130 GeV gamma-ray line*, *Phys.Rev.* **D86** (2012) 083525, [arXiv:1207.1468].

[22] X.-Y. Huang, Q. Yuan, P.-F. Yin, X.-J. Bi, and X.-L. Chen, *Constraints on the dark matter annihilation scenario of Fermi 130 GeV γ-ray line emission by continuous gamma-rays, Milky Way halo, galaxy clusters and dwarf galaxies observations*, *JCAP* **1211** (2012) 048, [arXiv:1208.0267].

[23] M. Asano, T. Bringmann, G. Sigl, and M. Vollmann, *The 130 GeV gamma-ray line and generic dark matter model building constraints from continuum gamma rays, radio and antiproton data*, arXiv:1211.6739.

[24] E. Dudas, Y. Mambrini, S. Pokorski, and A. Romagnoni, *Extra U(1) as natural source of a monochromatic gamma ray line*, *JHEP* **1210** (2012) 123, [arXiv:1205.1520].

[25] J. M. Cline, *130 GeV dark matter and the Fermi gamma-ray line*, *Phys.Rev.* **D86** (2012) 015016, [arXiv:1205.2688].

[26] H. M. Lee, M. Park, and W.-I. Park, *Fermi Gamma Ray Line at 130 GeV from Axion-Mediated Dark Matter*, *Phys.Rev.* **D86** (2012) 103502, [arXiv:1205.4675].

[27] B. Kyae and J.-C. Park, *130 GeV Gamma-Ray Line from Dark Matter Decay*, *Phys.Lett.* **B718** (2013) 1425–1429, [arXiv:1205.4151].

[28] X. Chu, T. Hambye, T. Scarna, and M. H. Tytgat, *What if Dark Matter Gamma-Ray Lines come with Gluon Lines?*, *Phys.Rev.* **D86** (2012) 083521, [arXiv:1206.2279].

[29] Z. Kang, T. Li, J. Li, and Y. Liu, *Brightening the (130 GeV) Gamma-Ray Line*, arXiv:1206.2863.

[30] J. H. Heo and C. Kim, *Cosmic ray signatures of Dipole-Interacting Fermionic Dark Matter*, arXiv:1207.1341.

[31] J.-C. Park and S. C. Park, *Radiatively decaying scalar dark matter through U(1) mixings and the Fermi 130 GeV gamma-ray line*, *Phys.Lett.* **B718** (2013) 1401–1406, [arXiv:1207.4981].

[32] N. Weiner and I. Yavin, *UV Completions of Magnetic Inelastic Dark Matter and RayDM for the Fermi Line(s)*, arXiv:1209.1093.

[33] K. Schmidt-Hoberg, F. Staub, and M. W. Winkler, *Enhanced diphoton rates at Fermi and the LHC*, *JHEP* **1301** (2013) 124, [arXiv:1211.2835].

[34] A. Sommerfeld, Annalen der Physik, 403, 257 (1931).

[35] J. Hisano, S. Matsumoto, and M. M. Nojiri, *Unitarity and higher-order corrections in neutralino dark matter annihilation into two photons*, *Phys. Rev.* **D67** (2003) 075014, [hep-ph/0212022].

[36] J. Hisano, S. Matsumoto, and M. M. Nojiri, *Explosive dark matter annihilation*, *Phys. Rev. Lett.* **92** (2004) 031303, [hep-ph/0307216].

[37] J. Hisano, S. Matsumoto, M. M. Nojiri, and O. Saito, *Non-perturbative effect on dark matter annihilation and gamma ray signature from galactic center*, *Phys. Rev.* **D71** (2005) 063528, [hep-ph/0412403].

[38] M. Cirelli, A. Strumia, and M. Tamburini, *Cosmology and Astrophysics of Minimal Dark Matter*, *Nucl. Phys.* **B787** (2007) 152–175, [arXiv:0706.4071].

[39] N. Arkani-Hamed, D. P. Finkbeiner, T. R. Slatyer, and N. Weiner, *A Theory of Dark Matter*, *Phys.Rev.* **D79** (2009) 015014, [arXiv:0810.0713].

[40] R. Iengo, *Sommerfeld enhancement for a Yukawa potential*, arXiv:0903.0317.

[41] R. Iengo, *Sommerfeld enhancement: general results from field theory diagrams*, *JHEP* **05** (2009) 024, [arXiv:0902.0688].

[42] S. Cassel, *Sommerfeld factor for arbitrary partial wave processes*, *J. Phys.* **G37** (2010) 105009, [arXiv:0903.5307].

[43] T. R. Slatyer, *The Sommerfeld enhancement for dark matter with an excited state*, *JCAP* **1002** (2010) 028, [arXiv:0910.5713].

[44] A. Hryczuk, R. Iengo, and P. Ullio, *Relic densities including Sommerfeld enhancements in the MSSM*, *JHEP* **1103** (2011) 069, [arXiv:1010.2172].

[45] J. B. Dent, S. Dutta, and R. J. Scherrer, *Thermal Relic Abundances of Particles with Velocity-Dependent Interactions*, *Phys.Lett.* **B687** (2010) 275–279, [arXiv:0909.4128].

[46] J. Zavala, M. Vogelsberger, and S. D. White, *Relic density and CMB constraints on dark matter annihilation with Sommerfeld enhancement*, *Phys.Rev.* **D81** (2010) 083502, [arXiv:0910.5221].

[47] J. L. Feng, M. Kaplinghat, and H.-B. Yu, *Halo Shape and Relic Density Exclusions of Sommerfeld-Enhanced Dark Matter Explanations of Cosmic Ray Excesses*, *Phys.Rev.Lett.* **104** (2010) 151301, [arXiv:0911.0422].

[48] J. L. Feng, M. Kaplinghat, and H.-B. Yu, *Sommerfeld Enhancements for Thermal Relic Dark Matter*, *Phys.Rev.* **D82** (2010) 083525, [arXiv:1005.4678].

[49] **PAMELA Collaboration** Collaboration, O. Adriani *et. al.*, *An anomalous positron abundance in cosmic rays with energies 1.5-100 GeV*, *Nature* **458** (2009) 607–609, [arXiv:0810.4995].

[50] J. Chang *et. al.*, *An excess of cosmic ray electrons at energies of 300-800 GeV*, *Nature* **456** (2008) 362–365.

[51] **Fermi LAT Collaboration** Collaboration, A. A. Abdo *et. al.*, *Measurement of the Cosmic Ray e+ plus e- spectrum from 20 GeV to 1 TeV with the Fermi Large Area Telescope*, *Phys.Rev.Lett.* **102** (2009) 181101, [arXiv:0905.0025].

[52] D. P. Finkbeiner, L. Goodenough, T. R. Slatyer, M. Vogelsberger, and N. Weiner, *Consistent Scenarios for Cosmic-Ray Excesses from Sommerfeld-Enhanced Dark Matter Annihilation*, *JCAP* **1105** (2011) 002, [arXiv:1011.3082].

[53] R. J. Scherrer and M. S. Turner, *On the Relic, Cosmic Abundance of Stable Weakly Interacting Massive Particles*, *Phys.Rev.* **D33** (1986) 1585.

[54] T. Bringmann and S. Hofmann, *Thermal decoupling of WIMPs from first principles*, *JCAP* **0407** (2007) 016, [hep-ph/0612238].

[55] T. Bringmann, *Particle Models and the Small-Scale Structure of Dark Matter*, *New J.Phys.* **11** (2009) 105027, [arXiv:0903.0189].

[56] **WMAP Collaboration** Collaboration, E. Komatsu *et. al.*, *Seven-Year Wilkinson Microwave Anisotropy Probe (WMAP) Observations: Cosmological Interpretation*, *Astrophys.J.Suppl.* **192** (2011) 18, [arXiv:1001.4538].

[57] M. Cirelli and J. M. Cline, *Can multistate dark matter annihilation explain the high-energy cosmic ray lepton anomalies?*, *Phys.Rev.* **D82** (2010) 023503, [arXiv:1005.1779].

[58] K. N. Abazajian and J. P. Harding, *Constraints on WIMP and Sommerfeld-Enhanced Dark Matter Annihilation from HESS Observations of the Galactic Center*, *JCAP* **1201** (2012) 041, [arXiv:1110.6151].

[59] E. Bertschinger, Astrophs.J. Suppl. 58, 39 (1985).

[60] J. F. Navarro, A. Ludlow, V. Springel, J. Wang, M. Vogelsberger, *et. al.*, *The Diversity and Similarity of Cold Dark Matter Halos*, arXiv:0810.1522.

[61] T. R. Slatyer, N. Toro, and N. Weiner, *Sommerfeld-enhanced annihilation in dark matter substructure: Consequences for constraints on cosmic-ray excesses*, *Phys.Rev.* **D86** (2012) 083534, [arXiv:1107.3546].

[62] P. B. Tissera, S. D. White, S. Pedrosa, and C. Scannapieco, *Dark matter response to galaxy formation*, arXiv:0911.2316.

[63] J. Hisano, M. Kawasaki, K. Kohri, T. Moroi, K. Nakayama, *et. al.*, *Cosmological constraints on dark matter models with velocity-dependent annihilation cross section*, *Phys.Rev.* **D83** (2011) 123511, [arXiv:1102.4658].

[64] E. Dudas, Y. Mambrini, S. Pokorski, and A. Romagnoni, *Extra U(1) as natural source of a monochromatic gamma ray line*, *JHEP* **1210** (2012) 123, [arXiv:1205.1520].

[65] N. Weiner and I. Yavin, *UV Completions of Magnetic Inelastic Dark Matter and RayDM for the Fermi Line(s)*, arXiv:1209.1093.

[66] A. Hryczuk, *The Sommerfeld enhancement for scalar particles and application to sfermion co-annihilation regions*, *Phys.Lett.* **B699** (2011) 271–275, [arXiv:1102.4295].

[67] A. Hryczuk and R. Iengo, *The one-loop and Sommerfeld electroweak corrections to the Wino dark matter annihilation*, *JHEP* **1201** (2012) 163, [arXiv:1111.2916].